EPJ manuscript No.
(will be inserted by the editor)

A Discrimination Procedure between Muon and Electron in Super-Kamiokande Experiment Based on the Angular Distribution Function Method

V.I. Galkin[1], A.M. Anokhina[1], E. Konishi[2], and A. Misaki[3]

[1] Department of Physics, Moscow State University,Moscow, 119992, Russia
[2] Graduated School of Science and Technology, Hirosaki University, 036-8561, Hirosaki, Japan
[3] Advanced Research Institute for Science and Engineering, Waseda University, 169-0092, Tokyo, Japan
e-mail:misaki@kurenai.waseda.jp

Received: date / Revised version: date

Abstract. In the previous paper, we construct the angular distribution functions for muon and electron as well as their relative fluctuation functions to find suitable discrimination procedure between muon and electron in Superkamiokande experiment. In the present paper, we are able to discriminate muons from electrons in Fully Contained Events with a probability of error of less than several %. At the same time, our geometrical reconstruction procedure, considering only the ring-like structure of the Cherenkov image, gives an unsatisfactory resolution for 1 GeV e and μ, with a mean vertex position error, δr, of 5–10 m and a mean directional error, $\delta\theta$, of about 6°–20°. In contrast, a geometrical reconstruction procedure utilizing the full image and using a detailed approximation of the event angular distribution works much better: for a 1 GeV e, $\delta r \sim$2 m and $\delta\theta \sim$3°; for a 1 GeV μ, $\delta r \sim$3 m and $\delta\theta \sim$5°. At 5 GeV, the corresponding values are $\sim$1.4 m and $\sim$2° for e and $\sim$2.9 m and $\sim$4.3° for μ. The numerical values depend on a single PMT contribution threshold. The values quoted above are the minima with respect to this threshold. Even the methodologically correct approach we have adopted, based on detailed simulations using closer approximations than those adopted in the SK analysis, cannot reproduce the accuracies for particle discrimination, momentum resolution, interaction vertex location, and angular resolution obtained by the SK simulations, suggesting the assumptions in these may be inadequate.

PACS. 13.15.+g Neutrino interactions – 14.60.-z leptons

1 Introduction

In the preceeding paper [1], we have proposed a new discrimination procedure between electron and muon in the SK experiment instead of the standard SK procedure. For the purpose, we have constructed the mean angular distribution functions for the charged particles concerned (muons and electrons/positrons), as well as the corresponding functions for the relative fluctuation. In the present paper, we apply our discrimination procedure to the SK experiment.

2 Procedure for discriminating electron neutrinos from muon neutrinos: Event type definition

Figure 1 shows the process of classification, i.e. how event is called mu-like (muon event) or e-like (electron event). First, one needs to calculate patterns for classes μ and e with the help of models of Cherenkov light spatial-angular distribution. Second, one should compare the event under consideration with both patterns by calculating q_μ (7-a) and q_{el} (7.b) which will be shown later (See page 2). Third, one compares their difference with q_{crit} thus making a decision on the type of event.

In order to discriminate electron neutrino events from muon neutrino events, we construct discrimination functions in the following way.

We consider each event to be a random vector $\mathbf{Q} = \{Q_j\}$ containing the contributions to all photomultipliers (PMTs) of the detector. Here j is the PMT index: $j = 1, 2, ..., N$ and N is the total number of PMT of the detector. There are two classes of events to be considered by the type identification procedure: $\omega_1 = e$ (electron initiated) and $\omega_2 = \mu$ (muon initiated). Monte Carlo simulations of event optical images provide a possibility to study the behaviour of images of both classes, namely, the image distribution functions $F(Q_1, Q_2, ..., Q_N; \omega_i, E_0, \mathbf{r_0}, \theta_\mathbf{0})$ which are simultaneous distribution functions of PMT contributions Q_j for given particle type ω_i, energy E_0, injection

Send offprint requests to:

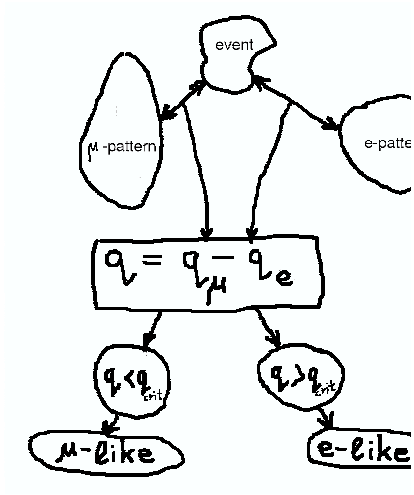

Fig. 1. schematic view of pattern recognition.

point $\mathbf{r_0}$ and direction $\theta_\mathbf{0}$. i.e. the most differential and complete characteristics of the classes.

It is, however, too expensive to deal with these functions: in principle, one should simulate an enormous sample to know the most differential distribution function even for only one set of primary parameters $\{\omega_i, E_0, \mathbf{r_0}, \theta_\mathbf{0}\}$. A more practical solution is to determine only the mean vector $\{\bar{Q}_j(\omega_i, E_0, \mathbf{r_0}, \theta_\mathbf{0})\}$ and the covariance matrix $\Sigma_Q(\omega_i, E_0, \mathbf{r_0}, \theta_\mathbf{0}) = cov(Q_j, Q_m)$ and then assume the distribution is a multi-variate normal one:

$$p(\mathbf{Q}; \omega_i, E_0, \mathbf{r_0}, \theta_\mathbf{0}) = (2\pi)^{-N/2} \cdot \left(det\, \Sigma_{\omega_i}^{-1}\right)^{-1/2} \times$$
$$\times exp\left\{-\left(\mathbf{Q} - \mathbf{Q}^{\omega_\mathbf{i}}\right)^T \Sigma_{\omega_i}^{-1} \left(\mathbf{Q} - \mathbf{Q}^{\omega_\mathbf{i}}\right)\right\}, \qquad (1)$$

Here
$\mathbf{Q}^{\omega_\mathbf{i}} = \mathbf{Q}(\omega_i, E_0, \mathbf{r_0}, \theta_\mathbf{0}), \Sigma_{\omega_i} = \Sigma_Q(\omega_i, E_0, \mathbf{r_0}, \theta_\mathbf{0})$.
In this case, one still needs a sufficiently large sample to calculate $\bar{\mathbf{Q}}$ and Σ_Q accurately.

Our approach assumes that one can calculate the mean image vector $\bar{\mathbf{Q}}$ and fluctuation vector $\delta\mathbf{Q}$ using the approximations of the Cherenkov light mean angular distributions and their fluctuations. Simulation shows that correlation coefficients of single PMT contributions amount to 0.6(0.8) for the neighbouring PMTs and go down to 0.1(0.1) for distant PMTs in electron(muon) events, which makes the covariance matrix diagonal-like.

Thus, we neglect all correlations between Q_j and the resulting normal distribution becomes simpler:

$$p(\mathbf{Q}; \omega_i, E_0, \mathbf{r_0}, \theta_\mathbf{0}) = (2\pi)^{-N/2} \cdot \left(\prod_{j=1}^{N} \delta Q_j^{\omega_i}\right)^{1/2}$$
$$\times exp\left\{-\sum_{j=1}^{N} \frac{\left(Q_j - Q_j^{\omega_i}\right)^2}{\delta Q_j^{\omega_i}}\right\}, \qquad (2)$$

For a certain event geometry (starting point $\mathbf{r_0}$ and direction $\theta_\mathbf{0}$ of the particle) and energy E_0 we calculate mean pattern images $Q_j^{\omega_i} = Q_j^{e,\mu}(E_0, \mathbf{r_0}, \theta_\mathbf{0})$ and their deviations $\delta Q_j^{\omega_i} = \delta Q_j^{e,\mu}(E_0, \mathbf{r_0}, \theta_\mathbf{0})$:

$$Q_j^{e,\mu}(E_0, \mathbf{r_0}, \theta_\mathbf{0})$$
$$= \sum_{k=1}^{n} \frac{S}{\rho_{j,k}^2} \cdot cos\chi_{j,k} \cdot exp\left(-\frac{\rho_{j,k}}{\lambda_{abs}}\right) \cdot F_k^{e,\mu}(\theta_{j,k}), \qquad (3)$$

$$\delta Q_j^{e,\mu}(E_0, \mathbf{r_0}, \theta_\mathbf{0}) = \sum_{k=1}^{n} \left[\frac{S}{\rho_{j,k}^2} \cdot cos\chi_{j,k} \cdot exp\left(-\frac{\rho_{j,k}}{\lambda_{abs}}\right)\right]^2$$
$$\times \left[F_k^{e,\mu}(\theta_{j,k}) \cdot \delta_k^{e,\mu}(\theta_{j,k})\right]^2, \qquad (4)$$

where k is the segment index, n is the number of segments in a track/shower, S is the PMT area, $\rho_{j,k}$ is the distance between a segment center and a PMT center(see Fig. 2), $\chi_{j,k}$ is the cosine of the angle between $\rho_{\mathbf{j,k}}$ and a PMT axis (which is normal to the tank surface), $\theta_{j,k}$ is the radiation angle from the segment center to the PMT center, and λ_{abs} is light absorption length in water. And $F_k^{e,\mu}(\theta_{j,k})$ is the mean angular distribution function, $\delta_k^{e,\mu}(\theta_{j,k})$ is its relative fluctuation.

Eq.(4) implies there are no correlations between the contribution from different segments of track/shower which is close to reality: in simulated electron event samples correlation coefficients between neighbouring segments do not exceed 0.4 and amount to 0.1 for distant segments. In muon events characteristic values of the coefficients between different segments (including neighbouring ones) are even smaller: 0.1; the exceptions are the trailing (last) segments which emit about 100 times less than the other ones but are tightly correlated due to the muon decay process.

Then we apply Bayes' decision rule which minimizes the error of misidentification assuming that prior probabilities of both types of events are equal:

$$r = \frac{P(e/\mathbf{Q})}{P(\mu/\mathbf{Q})} = \frac{p(\mathbf{Q}/e)}{p(\mathbf{Q}/\mu)} =$$
$$= \frac{\left(\prod_{j=1}^{N} \delta Q_j^e\right)^{1/2}}{\left(\prod_{j=1}^{N} \delta Q_j^\mu\right)^{1/2}} \cdot \frac{exp\left\{-\sum_{j=1}^{N} \left(Q_j - Q_j^e\right)^2 / \delta Q_j^e\right\}}{exp\left\{-\sum_{j=1}^{N} \left(Q_j - Q_j^\mu\right)^2 / \delta Q_j^\mu\right\}}, \qquad (5)$$

where $p(\mathbf{Q}/e)$ and $p(\mathbf{Q}/\mu)$ come from Eq.(2).

The simplest criterion, q, which we use to define the type of event is:

$$q = ln\, r = q_\mu - q_{el} + C, \qquad (6)$$

$$q_\mu = \sum_{j=1}^{N} \left(Q_j^{exp} - Q_j^\mu\right)^2 / \delta Q_j^\mu, \qquad (7-a)$$

$$q_{el} = \sum_{j=1}^{N} \left(Q_j^{exp} - Q_j^e\right)^2 / \delta Q_j^e, \qquad (7-b)$$

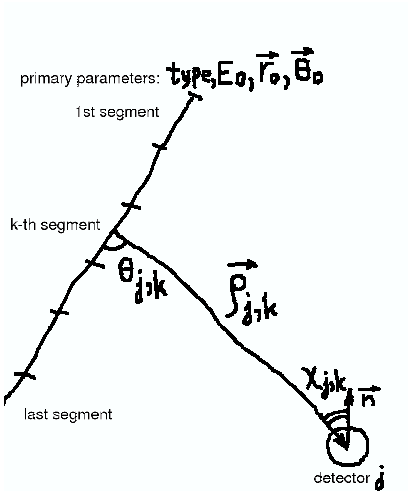

Fig. 2. geometry for eqs.3 and 4.

$$C \;=\; \frac{1}{2}\, ln\, \frac{\prod\limits_{j=1}^{N} \delta Q_j^e}{\prod\limits_{j=1}^{N} \delta Q_j^\mu}\;, \quad (7-c)$$

where Q_j^{exp} is the contribution to j-th PMT in the "experimental" image under consideration. The event is considered to be e-like if $q > 0$ and μ-like if $q < 0$.

A slightly more general form of the criterion can help to reduce the errors of type definition:

$$q \;=\; q_\mu \;-\; A \cdot q_{el} \;+\; B\;, \quad (8)$$

where A, B are tuned to minimize the identification errors; the usage is the same as above.

3 Examination of the procedure for discriminating electrons from muons

3.1 A virtual 1 kilo-ton water tank detector for the KEK experiment

As explained in the preceeding paper[1], the SK discrimination procedure was constructed on the following assumptions in the Kamiokande analysis – the predecessor to SK :

$$N_{i,exp}(direct) = \alpha_e \times N_{MC}(\theta_i, p_e) \times \left(\frac{16.9}{l_i}\right)^{\gamma}$$

$$\times \exp\left(-\frac{l_i}{L}\right) \times f(\Theta), \quad (9)$$

$$N_{i,exp}(direct) =$$

$$= \left\{\alpha_\mu \times \frac{1}{l_i(sin\theta_i + l_i \times (\frac{d\theta}{dx}))} \times sin^2\theta_i + N_{i,knock}(\theta_i)\right\} \times$$

$$\times \exp\left(-\frac{l_i}{L}\right) \times f(\Theta), \quad (10)$$

$$Prob = \frac{1}{\sqrt{2\pi}\sigma} \exp\left(-\frac{(N_{obs} - N_{exp})^2}{2\sigma^2}\right), \quad (11)$$

$$P_{pattern}(e) =$$

$$= \exp\left\{-\frac{1}{2}\left(\frac{\chi^2(e) - min[\chi^2(e), \chi^2(\mu)]}{\sigma_{\chi^2}}\right)^2\right\}, \quad (12-a)$$

$$P_{pattern}(\mu) =$$

$$= \exp\left\{-\frac{1}{2}\left(\frac{\chi^2(\mu) - min[\chi^2(e), \chi^2(\mu)]}{\sigma_{\chi^2}}\right)^2\right\}. \quad (12-b)$$

$$P_{angle}(e) =$$

$$= constant \times \exp\left\{-\frac{1}{2}\left(\frac{\theta_{exp}(e) - \theta_{obs}}{\Delta\theta}\right)^2\right\}, \quad (13-a)$$

$$P_{angle}(\mu) =$$

$$= constant \times \exp\left\{-\frac{1}{2}\left(\frac{\theta_{exp}(\mu) - \theta_{obs}}{\Delta\theta}\right)^2\right\}, \quad (13-b)$$

$$P(e) = P_{pattern}(e) \times P_{angle}(e), \quad (14-a)$$

$$P(\mu) = P_{pattern}(\mu) \times P_{angle}(\mu). \quad (14-b)$$

These expressions was given firstly in Takita [2].

However, in order to show the validity of this discrimination procedure which had never been confirmed by accelerator beam, the SK group performed an accelerator experiment using the KEK 12 GeV proton synchrotron (Kasuga[3], Kasuga et al.[4], Sakai[5], Kasuga[6]). For the confirmation, one kiloton water Cherenkov detector was constructed and the SK group studied the particle identification capabilities over the momentum range 250 MeV/c to 1000 MeV/c for muons and 100 MeV/c to 1000 MeV for electrons. They concluded that the particle misidentification probabilities with SK discrimination procedure is less than 1 to 5% (Sakai, p.141 [5], Kasuga, p.77 [6]). Based on these procedures, the SK group have reported experimental results which have lead to the claimed existence of neutrino oscillations. To study the positional dependence of the discrimination, data was taken for 10 injection points in the 1-kiloton detector: WUS, ESS, WUC, WUD, ... (See Sakai[5] in detail). We have constructed a virtual 1 kiloton water Cherenkov detector, including the same PMT configuration, as the SK test one in our computer. In the virtual detector we simulate physical events and examine the influence of the virtual physical events on the virtual detector.

In Figure 3 we give the relation between the emitted Cherenkov light and the detected Cherenkov light for

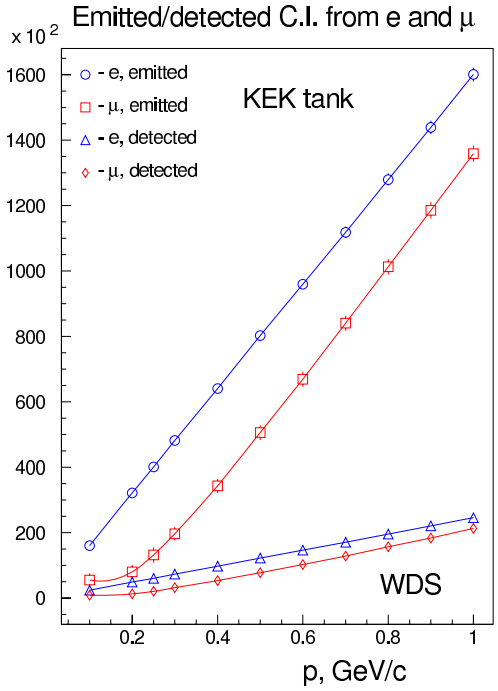

Fig. 3. The average behavior of the Cherenkov light for both emitted and detected as the functions of momentum for muons and electrons which are generated at WDS.

the WDS injection point (see Sakai's paper). The emitted Cherenkov light denotes the total Cherenkov light produced by the charged particle concerned, while the detected light records only that which is measured by the detector. This relation holds almost exactly, irrespective of the generation point, because the absorption length is so large compared with the dimensions of the 1 kilo-ton detector.

It is clear from Figure 3 that there is big difference as for the Cherenkov light quantity between the emitted Cherenkov light and the detected one. The emitted Cherenkov light denotes, by the definition , the total Cherenkov light, while the detected Cherenkov light denotes only small part of the emitted one. Consequently, we expect variety of the patterns of the detected Cherenkov lights for the events concerned due to the PMT configuration.

Using the discrimination procedure developed in section 2 (Eq.(8), A=1, B=q_{crit}), we try to discriminate 300 MeV electrons from 500 MeV muons, both of which result, on average, in the production of the same amount of Cherenkov light. The result is given in Figure 4. As can be seen, discriminating between the electron and muon seems to be very difficult. In Table 1 we give misidentification probability for different q_{crit}. The parameter q_{crit} denotes a criterion for discriminating between muons and electrons: $e \rightarrow \mu$ denotes the probability for an electron to be misidentified as a muon, and $\mu \rightarrow e$ denotes the probability for a muon to be misidentified as an electron. It is easily understood from Figure 4 that a non-negligible number of muon events penetrate into the electron events

Table 1. Misidentification probability between 300MeV electron events and 500MeV muon events in the virtual KEK 1 kiloton tank detector, taking into account forward scattering only.

run	q_{crit}	$e \rightarrow \mu$ %	$\mu \rightarrow e$ %
1	-4.00e2	1.67	25.67
2	-5.00e2	2.67	22.33
3	-6.00e2	6.67	19.67
4	-7.00e2	12.67	18.67
5	-8.00e2	20.33	17.30
6	-9.10e2	27.33	15.67
7	-1.00e3	35.67	12.67

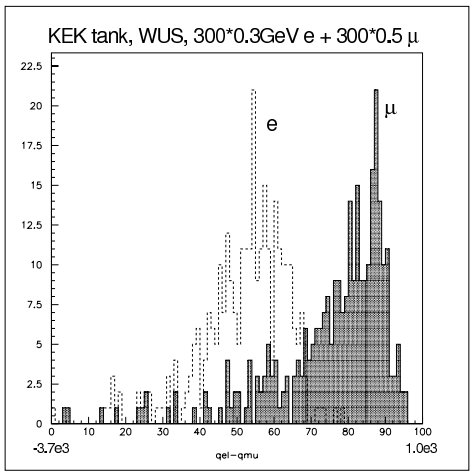

Fig. 4. The q_{el}-q_{μ} distribution for simulated events for 300 MeV electrons and 500 Mev muons in the KEK kiloton tank with angular distribution function describing only the forward hemisphere. These particles produce approximately the same amount of Cherenkov light. The notation " 300*0.3 GeV e " denotes the reslutls for 300 MeV electrons from 300 simulations.

region, so that some muon events may be misidentified as electrons.

Thus, we carefully examined the muon events which were located in the electron event parameter space, i.e., where electron events are found with high probabilities. As a result, we found that the majority of such muon events are $\mu - e$ decay events which should be identified as muon events. However, from the view point of the pattern recognition, we could not recognize whether the events in the gray zone between the 'clearly electron events' and the 'clearly muon events' were electrons or muons. To resolve this, we extend our angular distribution function, which was defined only within the forward hemisphere, to include the backward hemisphere and redefine q_{el} and q_{μ} in accordance with this extension.

Table 2. Misidentification probability between 300MeV electron events and 500MeV muon events in the virtual KEK 1 kiloton tank detector, taking into account forward and backward scattering.

run	q_{crit}	$e \rightarrow \mu$ %	$\mu \rightarrow e$ %
1	2.00e2	0.00	4.67
2	1.00e2	0.33	3.67
3	0.00	0.67	3.00
4	-1.00e2	0.67	2.00
5	-2.00e2	2.00	2.00
6	-3.10e2	3.67	2.00
7	-4.00e2	12.00	2.00
8	-5.00e2	20.33	1.67
9	-6.00e2	30.00	1.67
10	-7.00e2	43.67	1.33

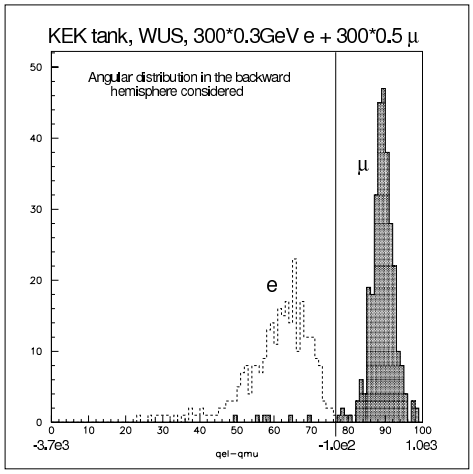

Fig. 5. The q_{el}-q_{μ} distribution for simulated events for 300 MeV electrons and 500 Mev muons in the KEK kiloton tank with angular distribution function describing both forward and backward hemisphere. These particles produce approximately the same amount of Cherenkov light. The notations are the same as for Figure 4.

After such a manipulation, one gets much smaller contamination of electron domain by muon events.

In Figure 5, we give the revised q_{el}-q_{μ} distribution where there is almost no intersection between the muon events and electron events. In Table 2, we give the misidentification probability based on the revised procedure. Comparing Table 2 with Table 1, we find that misidentification probability has decreased remarkably.

The probability distribution of the standard SK estimator for particle identification, if it were assumed to be remotely comparable, should be compared to Figure 4, not Figure 5, because the effect of $\mu - e$ decay was not considered correctly in the SK simulation (See Sakai,p.154, [5]). There are, thus, big differences between our result and the SK results (For example see Figure 3 in Sakai[5]). Namely, our initial result (Figure 4) could not reliably separate electron events from muon events, although it is claimed the standard SK analysis separates electron events from muon events almost completely. We can not imagine such a complete discrimination could be realized by the SK procedure.

The big difference between the "complete" discrimination by the SK (Figure 3 in Kasuga et al.[4]) and the poorer discrimination obtained by us (Figure 4) extends further, if we take into consideration the uncertainties added by the real detector to our Figure 4. This is because we do not consider the effect of photoelectrons produced from the parent Cherenkov light, which obeys a stochastic physical process, or the effect of scattered Cherenkov light. These two factors must increase the uncertainties in the discrimination between muons and electrons.

3.2 Discrimination of electrons from muons in the Super-Kamiokande detector in our simulation

Also, we have constructed a virtual SK detector incorporating the actual PMT configuration and have carried out the experiment numerically in our virtual SK detector. Based on the revised procedure for the discrimination of electron events from muon events developed in the previous section, we have discriminated electron events from muon events.

In Figure 6 we give the discrimination of the muon events from electron events in the virtual SK detector by the revised method. We conclude that we could discriminate muon events from electron events using the revised method with high probability. In Figure 7 we show the scatter plot between q_e and q_{μ}. From Figure 6 and Figure 7, we can conclude that our procedure for the discrimination of electron events from muon events works well.

In Figure 8 and Figure 10 we show the discrimination of muon events from electron events for a comparison of 500 MeV electrons with 700 MeV muons, and 700 MeV electrons with 900 MeV muons, respectively. These electron and muon energies were chosen as they yield roughly the same amount of Cherenkov light.

Also, scatter plots corresponding to Figure 8 and Figure 10 are given in Figure 9 and Figure 11, respectively. Comparing Figure 6 with Figure 8, it is apparent that the latter allows a better discrimination. Comparing Figure 8 with Figure 10, the latter is also better than the former for discrimination. The reason for this is that the generation of Cherenkov light for muon events becomes more different from that of the electron as their primary energies increase. Discrimination procedures of muon events from electron events in the SK detector are examined for events whose primary particles start at the "scaled WUS" position (x_0=986 cm, y_0=0 cm, z_0=282 cm, $\theta = \pi/2$and $\varphi = 0$).

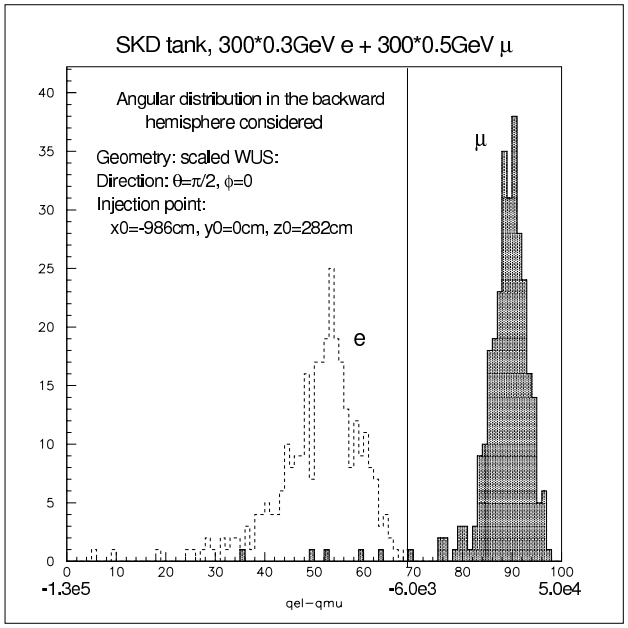

Fig. 6. The q_{el}-q_{μ} distribution for simulated events for 300 MeV electrons and 500 MeV muons in the virtual SK detector. The notations are the same as for Figure 4.

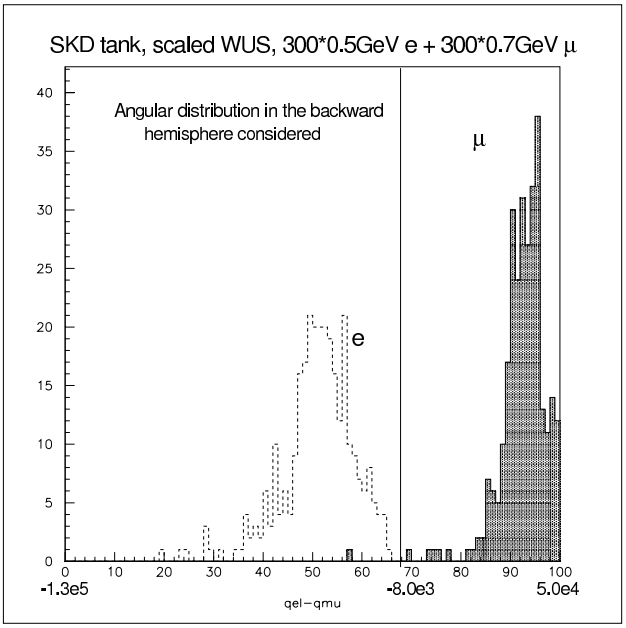

Fig. 8. The q_{el}-q_{μ} distribution for simulated events for 500 MeV electrons and 700 MeV muons in the virtual SK detector. The notations are the same as for Figure 4.

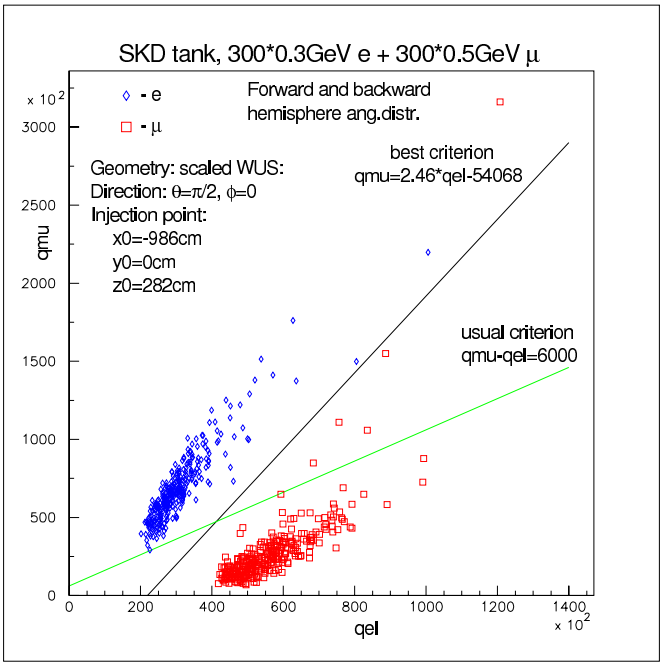

Fig. 7. The scatter plot for q_{el} and q_{μ} for 300 MeV electrons and 500 MeV muons considered in Figure 6.

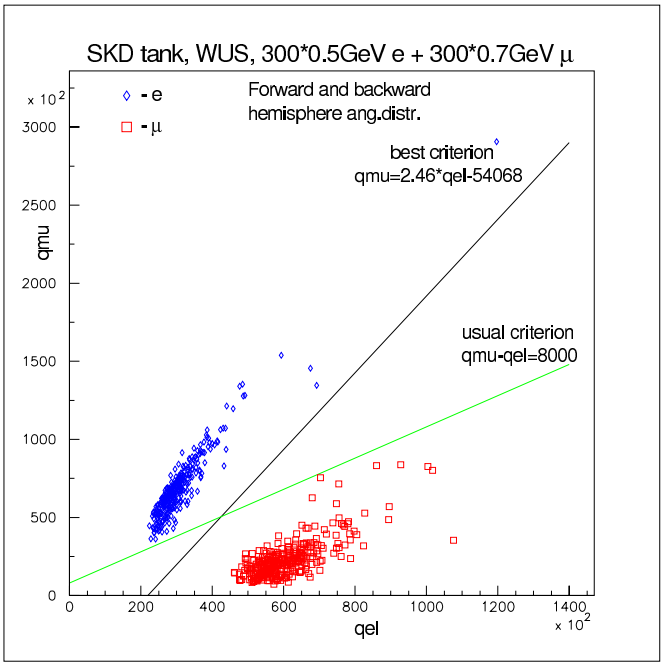

Fig. 9. The scatter plot for q_{el} and q_{μ} for 500 MeV electrons and 700 MeV muons considered in Figure 8.

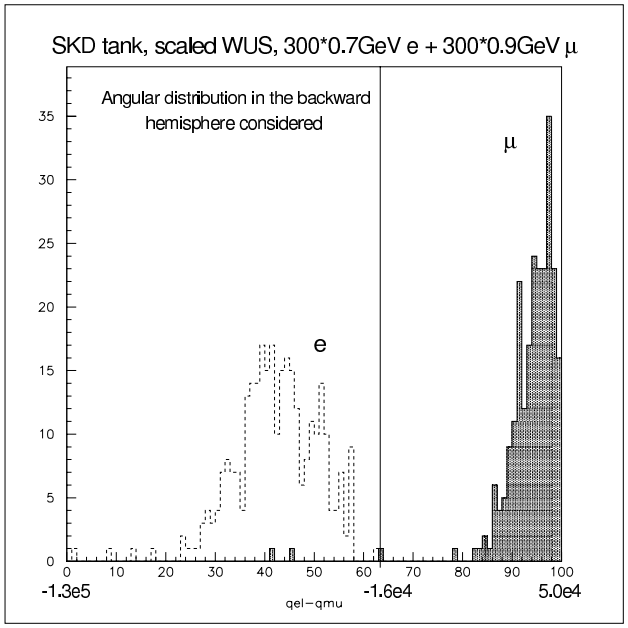

Fig. 10. The q_{el}-q_{μ} distribution for simulated events for 700 MeV electrons and 900 MeV muons in the virtual SK detector. The notations are the same as for Figure 4.

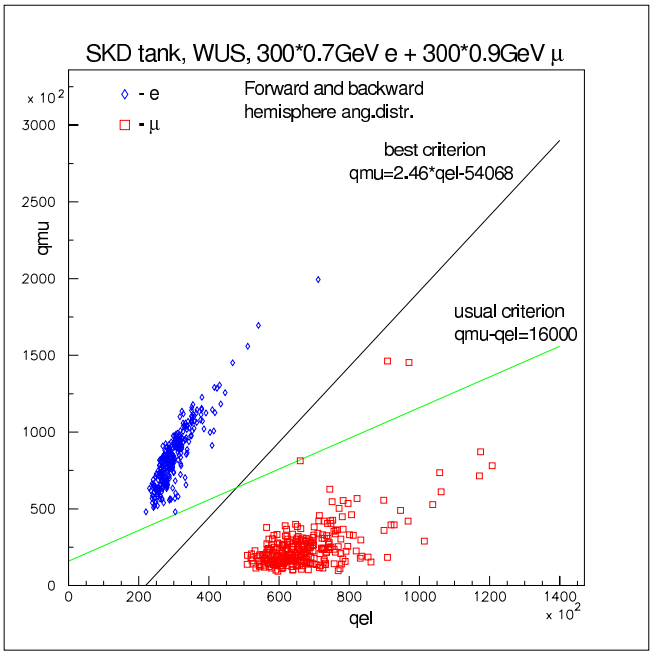

Fig. 11. The scatter plot for q_{el} and q_{μ} for 700 MeV electrons and 900 MeV muons considered in Figure 10.

4 Error Distribution for the vertex point and direction for muon and electron events

4.1 TDC procedure

The SK analysis introduces a "TDC procedure" to determine the vertex position. The principle of the TDC procedure is to find the position where the time residuals, t_i, for the PMTs being fitted are minimized. The time residual t_i of the i-th PMT is defined as

$$t_i = t_i^0 - \frac{n}{c} \times \sqrt{(x - x_i)^2 + (y - y_i)^2 + (z - z_i)^2}\,, \quad (15)$$

where t_i^0 is the hit time of the i-th PMT, (x_i, y_i, z_i) is the position of the i-th PMT, (x, y, z) is the effective emitting point position and c/n is the velocity of the Cherenkov light in water. That all the light is emitted from the same *effective* point in space and comes to j-th PMT *exactly* at the moment corresponding to the mean time $\bar{t_j}$ of the j-th PMT Cherenkov pulse is not really true. A simple equation for time residual used in a χ^2-like sum (the system of linear equations for the effective point coordinates (x^*, y^*, z^*) is overdefined!) can give effective point estimate after the sum's minimization (with respect to (x^*, y^*, z^*)) even if the original assumption is not valid. The effective point thus deduced does not coincide with the center-of mass of the light emitting system (e-shower or μ-track) because of specific mechanism of Cherenkov pulse formation and will usually differ from the event starting (injection) point.

The TDC procedure based only on $\bar{t_j}$ cannot estimate the event direction because to define a direction one needs at least two points. Direction estimates could be obtained as a result of Cherenkov pulse shape analysis for each sufficiently illuminated optical module if the PMT and electronics are fast enough for such analysis.

Sakai shows the time residual distribution of typical event (a 1 GeV/c, electron) which is distributed over 50 nanoseconds (Sakai, p.38 [5]), assuming a point-like source. We simulate the Cherenkov light in the cascade shower using GEANT 3.21 and the tools we have developed. In Figure 12 we give one example for the time residual distribution for a 1 GeV primary electron based on Eq.(15) with the use of the detailed simulation of the cascade shower. In our calculation, we simulate shower particles and the accompanying Cherenkov light due to shower particle concerned in an exact way. Then, we know the starting point of the primary electron. Shifting the starting point from the real point to a range of artificial ones, we can obtain the time residual distribution for each position, and examples are given in Figure 12.

Among the five different starting points, which includes the true one, the smallest standard deviation is obtained in the case of $Z' = Z + 100$ (cm), where Z' and Z denote the assumed vertex point and the real vertex point, respectively. Thus, the apparently most probable vertex point is not real one, but is offset by 100 cm from the real one. Of course, this is only one example and not average behavior. However we examined many individual cases and confirm that this is usual character which should hold even for the average behavior.

The comparison of our simulations with the experimental data from the SK experiment (Sakai) reveals a large difference. The width of our time residuals distribution is within one nanosecond, while the width for SK is ∼50 nanoseconds. The probable reasons are that we have

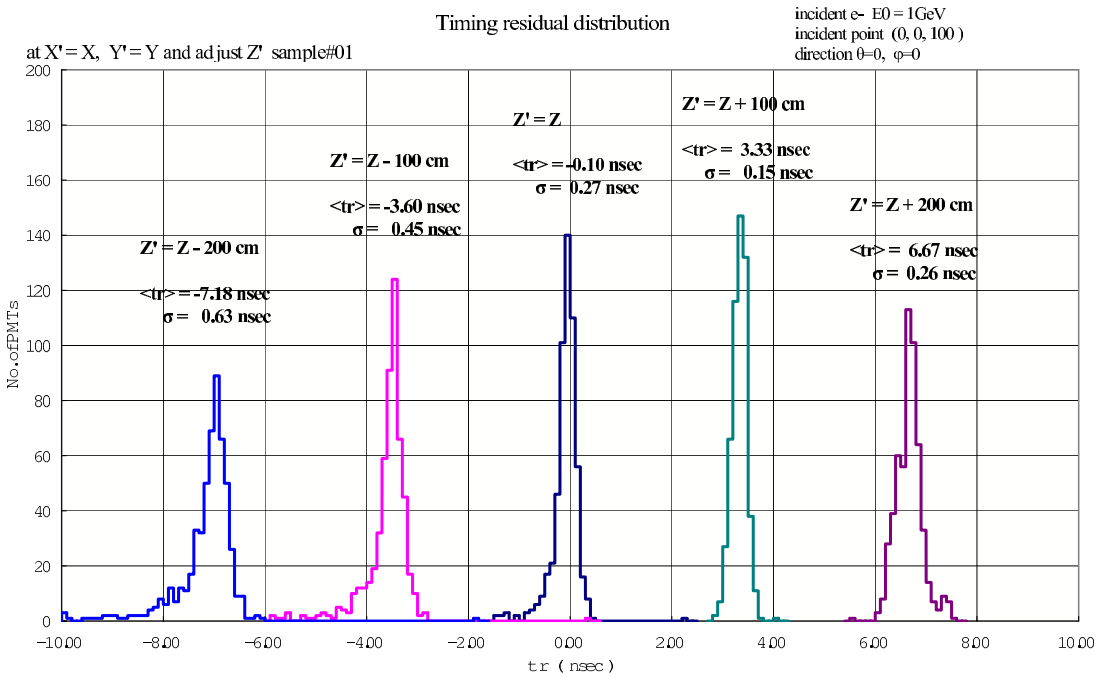

Fig. 12. One example of the time residual distributions for 1 GeV electron primary shower, assuming different vertex positions.

not considered the PMT and electronics response functions, and that we have neglected light scattering.

We calculate the time residuals for electrons of 500 MeV, 1 GeV, 3 GeV and 5 GeV, assuming that all Cherenkov light comes from certain points of a shower/track. From these calculations one can see that the smallest time residuals do not give the vertex position but yield points shifted from the vertex point along the direction of the cascade shower, namely, 50 to 100 cm for 500 MeV electrons, 100 to 150 cm for 1 GeV (Figure12) and 3 GeV electrons, and 150 to 200 cm for 5 GeV electrons. Such a tendency is quite understandable if we consider the size of the shower/track: the effective point should not be too close to the starting or ending points. The error of effective point location by minimizing the width of the distribution amounts to about 50 cm.

From the much larger width of the SK time residual distribution it is clear that in experimental conditions the effective point location error should be a few times greater because the minimum of the width as a function of effective point position would be much less pronounced.

For reasons mentioned above, we conclude that the SK TDC procedure is not suitable for the determination of an accurate vertex position for electron events. The situation for the muon events is essentially the same but must be worse than in the case of electron events as muon events have a longer extent than the corresponding electron events.

4.2 ADC procedure

The standard SK analysis uses an "ADC procedure" for event geometry reconstruction which is based only on the total amount of Cherenkov light detected by the PMTs.

We have constructed and used an ADC procedure which is based on the more detailed model for the angular distribution for the Cherenkov light described above.

4.2.1 Fundamental procedure for the error distribution for muon events and electron events: event geometry definition procedure

Our geometry reconstruction procedure assumes the type and energy of event are known. Thus, we only need to determine the event starting point $\mathbf{r_0}$ and the direction of the primary particle $\theta_\mathbf{0}$.

The first step is to find a ring-like (or arc-like) structure in the image. In muon events we observe two ring-like structures because the muon-decay electron produces a ring-like or a spot-like structure of its own, however, we do not consider muon energies below 500 MeV, so in muon events we choose the most intensive ring-like structure. This task is accomplished by row-by-row (or column-by-column) scanning of the arrays, representing an image, for maxima above a certain threshold.

The second step is defining the first approximation $\mathbf{r_1}, \theta_\mathbf{1}$ of geometrical parameters by fitting a ring structure with the following simple (cone-like) model: all light Q_{tot} emitted by a μ-track/e-shower is assumed to come from one effective point W on the track with the angular distribution of light being Heaviside-like:

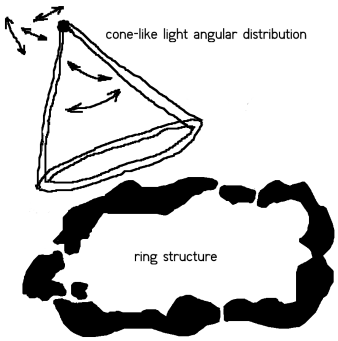

Fig. 13. 'cone' figure.

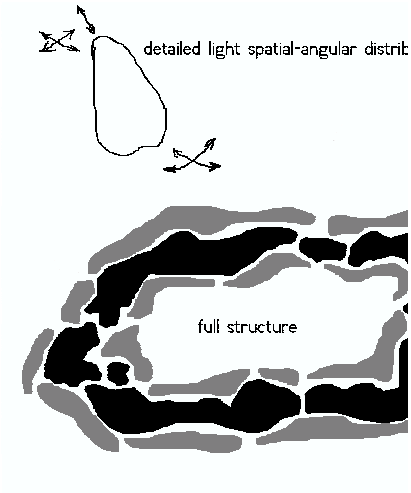

Fig. 14. 'full' figure.

$$F(\theta) \;=\; \begin{cases} 0, \;\theta \;<\; \bar{\theta} - \Delta\theta \\ a, \;|\theta - \bar{\theta}| \leq \Delta\theta \\ 0, \;\theta \;>\; \bar{\theta} + \Delta\theta \end{cases} \;,$$

$$a: \;\; 2\pi \int\limits_0^{\pi} F(\theta)\, sin\theta d\theta \;=\; Q_{tot} \quad (16)$$

The zero approximation for geometry parameters could be arbitrary because the ring-like structure is usually very pronounced and we use the cone-like model of Cherenkov light angular distribution with abrupt edges, the function to minimize with respect to $\mathbf{r}, \theta$ is:

$$G(\mathbf{r},\theta) \;=\; \sum_{l=1}^{M} \frac{\left(Q_l^{\,exp}(\mathbf{r_0},\theta_0) \;-\; Q_l(\mathbf{r},\theta)\right)^2}{Q_l^{\,exp}(\mathbf{r_0},\theta_0)} \;, \quad (17)$$

where l is the PMT index within the ring structure, M is the number of PMTs in the ring structure, $Q_l^{\,exp}(\mathbf{r_0},\theta_0)$ is the contribution to lth PMT from the event under consideration, $Q_l(\mathbf{r},\theta)$ is an estimate for this contribution calculated with the cone-like angular distribution model described above, $F(\theta)$:

$$Q_l(\mathbf{r},\theta) \;=\; \frac{S}{\rho_{l,W}^2} \cdot cos\chi_{l,W} \cdot exp\left(-\frac{\rho_{l,W}}{\lambda_{abs}}\right) \cdot F(\theta_{l,W}) \;, \quad (18)$$

The third and final step is the improvement of geometry parameter estimates by fitting all of the image above a certain threshold, Q_{thr}, with the pattern image $\{Q_j(E_0,\mathbf{r},\theta), \delta Q_j(E_0,\mathbf{r},\theta)\}$ calculated using the detailed model of Cherenkov light angular distribution. The previous step fit result $\mathbf{r_1}, \theta_1$ is used as the first approximation, and the function to minimize with respect to $\mathbf{r}, \theta$ is:

$$H(\mathbf{r},\theta) =$$

$$= \sum_{j:\, Q_j^{exp} \geq Q_{thr}} \frac{\left(Q_j^{exp}(E_0,\mathbf{r_0},\theta_0) \;-\; Q_j(E_0,\mathbf{r},\theta)\right)^2}{\delta Q_j(E_0,\mathbf{r},\theta)} \quad (19)$$

The PMT contribution threshold, Q_{thr}, could be optimized with respect to the resulting geometry parameter resolution, as we show later. The optimal threshold, $Q_{thr,\,opt}$, increases with primary energy, which could be used to enhance the resolution, because an estimate of the primary energy can be obtained from the total amount of Cherenkov light detected quite independently of the ADC procedure.

Figure 13 shows the process of geometry reconstruction using ring structure. Assuming geometry parameters of an event to be $\mathbf{r}, \theta$, cone-like angular distribution of light (Eq.(16)) is used to evaluate contributions (18) to all detectors (PMTs) of the ring structure in order to calculate $G(\mathbf{r},\theta)$ (Eq.(17)) which compares this rough light pattern with the light ring structure. Adjusting $\mathbf{r}$ and θ (see arrows in the figure) so that G approaches its minimum one obtains a rough estimate of the true geometry parameters $\mathbf{r}_0, \theta_0$.

Figure 14 shows the process of geometry reconstruction using full light image of an event. Assuming geometry parameters of an event to be $\mathbf{r}, \theta$ (for instance, these are values obtained in ring structure processing), the model of spatial-angular distribution of light is used to evaluate pattern image $\{Q_j(E_0,\mathbf{r},\theta), \delta Q_j(E_0,\mathbf{r},\theta)\}$ which is then used to calculate $H(\mathbf{r},\theta)$ (Eq.(19)) which compares it with the full light image of the event. Adjusting $\mathbf{r}$ and θ (see arrows in the figure) so that H approaches its minimum one obtains a better estimate of the true geometry parameters $\mathbf{r}_0, \theta_0$.

4.2.2 Application of the technique to simulated events

By using the technique developed in the previous section, we analyze simulated events to determine the error distributions for the vertex position and for the particle direction. Here, we examine the error distributions for 300 MeV electrons and 500 MeV muons, which yield roughly the same amount of Cherenkov light.

In Figure 15, we give the error distribution for the vertex position for 300 MeV electrons for different Cherenkov threshold quantities. "Ring only" denotes that only the

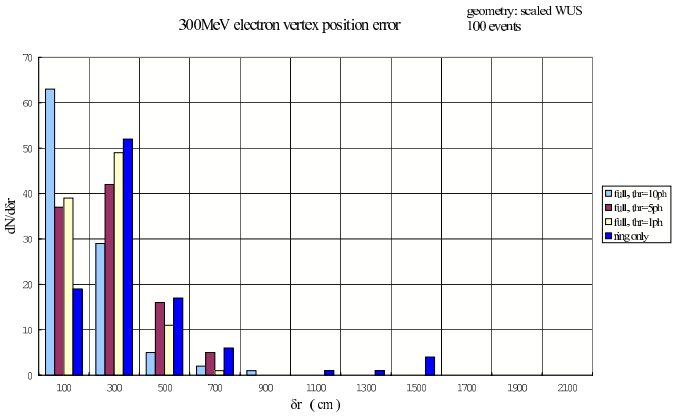

Fig. 15. Error distribution for the vertex position for 300 MeV electrons from the injected scaled WUS. The number of simulation is 100.

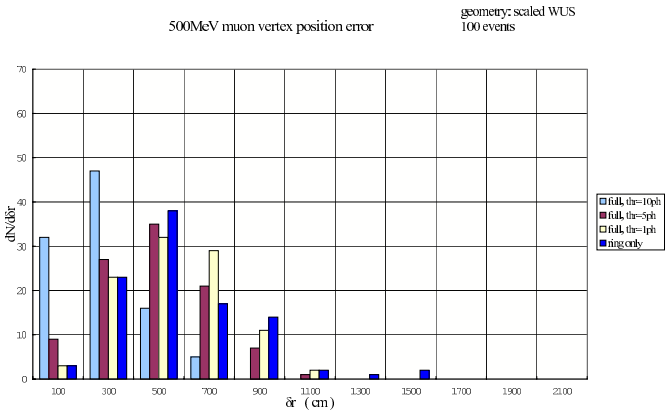

Fig. 16. Error distribution for the vertex position for 500 MeV muons from the injected scaled WUS. The number of simulation is100.

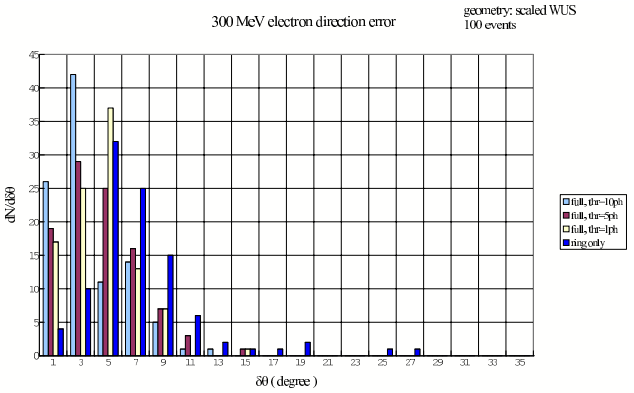

Fig. 17. Error distribution for the direction for 300 MeV electrons from the injected scaled WUS. The number of simulation is 100.

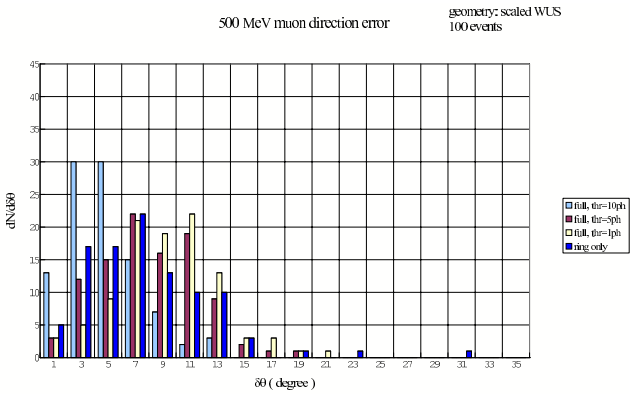

Fig. 18. Error distribution for the direction for 500 MeV muons from the injected scaled WUS. The number of simulation is 100.

information from PMTs whose Cherenkov photons contribute to the Cherenkov ring are used for the estimation of the error. "Full proc., thr=1ph" denotes that information from "ring only" PMTs and also those exceeding 1 Cherenkov photon are utilized for the estimation on the error. For "full proc., thr=5" and "full proc., thr=10", this latter threshold is raised to 5 and 10 photons, respectively.

In Figure 16 the error distribution for the vertex position for 500 MeV muons are given. It is clear that a wider error distribution is obtained for a "ring only" analysis. A narrower error distribution results from the "full proc, thr=10 ph" algorithm. This is the same as in the case of the electron. However, muons generally have wider error distributions than electrons: the mean error for 500 MeV muons for the vertex determination in the full analysis is 2.9 m while for 300 MeV electrons it amounts to 2 m.

In Figure 17, the error distribution for the direction of the 300 MeV electron is given. As expected, "ring only" gives the largest uncertainty distribution, while "full proc., thr=10ph" has the narrowest error distribution, with a mean error of about 3.7°. In Figure 18, we give the corresponding distributions for muons. The same trend is seen as for electrons, though the muons have a wider uncertainty distribution. The mean direction uncertainty in the best case is 4.9°.

Now, we compare 1 GeV electrons with 1 GeV muons, both of which yield roughly the same quantity of Cherenkov light. In Figure 19, we give the error distribution for the vertex position for 1 GeV electrons in the case of "full proc,thr=10". The mean error is 1.9 m. In Figure 20, the corresponding quantities for the muon are plotted. The average error for the vertex position is 3.2 m. Again, the error of the vertex point for muons is larger than for electrons.

In Figure 21, the error distribution for the direction for 1 GeV electron is shown. The average direction error is 3.0° for "full proc,thr=10". The corresponding quantities for the muon are plotted in Figure 22, where the mean error is 5.3°. Once again, the directional error for muons is larger than that for electrons.

In Table 3, we summarize the error distributions for the vertex points and the direction for both electrons and muons. Both mean errors and root mean square errors are given. Errors are also given for the different criteria,

Table 3. Mean and standard deviation of the error in the vertex position and the direction due to primary electrons and primary muons. These are given for different criteria for the Cherenkov threshold. Ring proc. denotes errors estimated using the Cherenkov ring only. [1], [5], [10], [20] denote errors estimated by the combination of [ring proc.] with a Cherenkov photon threshold of 1, 5, 10 and 20photons, respectively. Alm denotes the mean direction error in degrees. Als denotes the standard deviation for the corresponding mean values. Rm denotes the mean position error in metres. Rs denotes the standard deviation for the corresponding mean values.

		threshold				
		Ring proc.	[1]	[5]	[10]	[20]
300 MeV electron	Alm (deg.)	7.2	4.4	4.6	3.7	
	Als (deg.)	4.2	2.4	2.7	2.5	
	Rm (m)	3.88	2.50	2.74	1.98	
	Rs (m)	2.91	1.26	1.60	1.49	
500 MeV muon	Alm (deg.)	7.8	9.3	8.0	4.9	
	Als (deg.)	4.7	3.7	3.6	2.7	
	Rm (m)	5.71	5.69	4.92	2.94	
	Rs (m)	2.57	2.01	2.17	1.54	
1 GeV electron	Alm (deg.)	11.7	3.1		3.0	3.7
	Als (deg.)	14.4	3.5		3.7	4.4
	Rm (m)	6.49	1.99		1.86	2.17
	Rs (m)	8.21	2.19		2.24	2.55
1 GeV muon	Alm (deg.)	8.8	7.3		5.3	4.9
	Als (deg.)	11.3	11.1		10.0	10.0
	Rm (m)	5.98	4.25		3.15	2.70
	Rs (m)	6.76	4.92		3.99	3.62
5 GeV electron	Alm (deg.)	21.3			2.0	1.9
	Als (deg.)	11.0			5.1	4.4
	Rm (m)	15.07			1.43	1.32
	Rs (m)	6.65			2.76	2.66
5 GeV muon	Alm (deg.)	8.5			4.3	3.8
	Als (deg.)	6.7			4.0	3.8
	Rm (m)	4.68			2.89	2.45
	Rs (m)	2.52			2.55	2.45

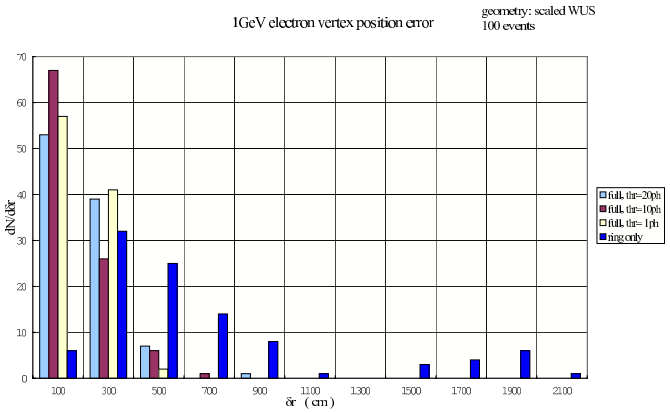

Fig. 19. Error distribution for the vertex position for 1 GeV electrons from the injected scaled WUS. The number of simulation is 100.

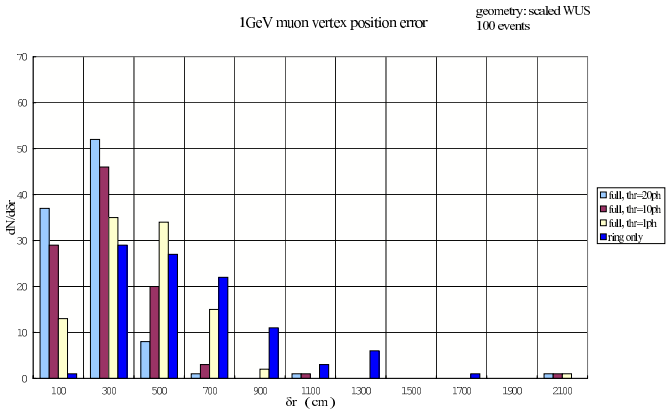

Fig. 20. Error distribution for the vertex position 1 GeV muons from the injected scaled WUS. The number of simulation is 100.

namely, different Cherenkov light threshold. From Figures 15 to 18 and Figures 19 to 22 and Table 3, it should be noticed the followings:

1. Of the different criteria considered, the "ring only" procedure results in the largest error. The reasons are as follows: The concept of the ring structure is essentially fuzzy, both in our procedure and the SK procedure, and information from ring structure is only part of the total information available for the pattern recognition. It is, therefore, natural that the vertex position and directional errors are largest in the "ring only" analysis. The standard SK analysis uses ring structure

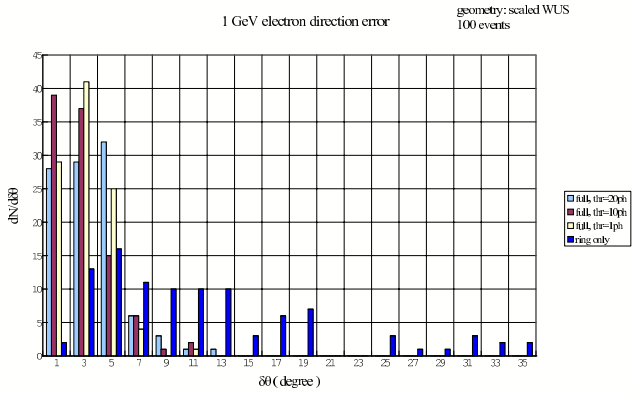

Fig. 21. Error distribution for the direction for 1 GeV electrons from the injected scaled WUS. The number of simulation is 100.

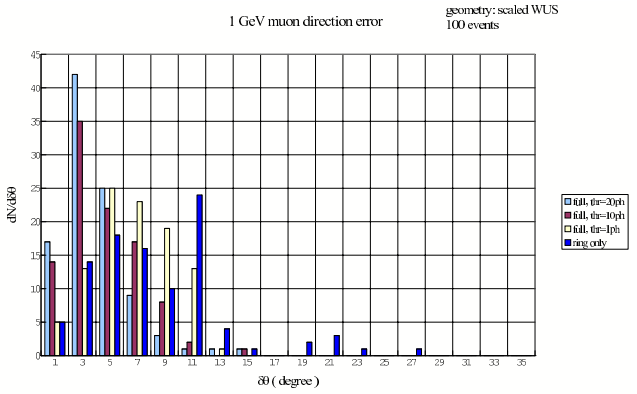

Fig. 22. Error distribution for the direction 1 GeV muons from the injected scaled WUS. The number of simulation is 100.

only, and their errors are amplified by that fact that the analysis ignores fluctuation effects.

2. Muons events have larger uncertainties than electron events. For both electrons and muons, the sources for the Cherenkov light are not point-like and have some extent in both cases. Significant errors come from the point-like approximation for electron events.
3. The optimal Cherenkov threshold for the third step of geometry reconstruction procedure depends on the primary energy of the particle concerned. For energies less than 1 GeV, third step with 10 photon threshold gives the best results for both muons and electrons among the alternatives considered. For 5 GeV electrons and muons, 20 photon threshold seems to be optimal for the third step.
4. The fact that the uncertainties for the determination of the vertex point and direction are rather large comes from the effect of fluctuations, namely the nature of the stochastic process concerned (an electron cascade shower or sequence of muon interactions with the medium). The utility of model developed in this paper, the moving point approximation model, is guaranteed, because it gives mean values and relative fluctuations precisely and takes all necessary geometrical considerations into account correctly. Even if additional errors exist, they should be negligible compared to the uncertainty caused by fluctuations. The rather large errors for the vertex point and the direction obtained by our model could not be reduced substantially, reflecting the essential nature of the physical processes concerned.
5. The SK analyses, according to all published accounts, completely neglect fluctuations and also use point-like approximations for the electron cascade. Moreover, they neglect the scattering effects on muon track geometry. As we showed earlier, their simple approximations distort the mean values in certain parameter domains. The most probable reason for their low error estimates is the fact that they completely neglect fluctuations in the event development. Our results contradict clearly the fine positional resolution of 23 to 56 cm claimed by for the SK analysis (Kibayashi, p.73[7]).
6. It should be noticed that errors derived by us are lower limits. As already mentioned, we do not consider the production of photoelectrons in PMTs, and only consider direct Cherenkov photons in our discrimination procedures neglecting the diffusion of Cherenkov photons. If we include these factors in our procedure, then, the actual errors for the vertex position and the direction should be larger than that given here.
7. Here, we make remarks to the results obtained by Mitsui et al([8]. They have calculated photoelectrons from the Cherenkov light due to both muon-like events and electron like events in the SK experiment by full Monte Carlo Method and have showed the clear deviation of the photoelectrons concerned from the Poisson distribution which SK assume(See,Eq.(11) in the present paper). Further, they have calculated PID parameter values following the SK PID methods which consists of the pattern and opening angles of the Cherenkov light. As the resluts of it, they have concluded that the total misidentification for muon and electron events is larger than or equal to 20 percent in sub-Gev and also at several percent in multi-GeV region. They attribute the deviation from the Poisson distribtuion to the neglect of the fluctuation from the stochastic proceeses inherent in electron-like eventsand muon-like events. We agree to their interpretation. However, we are forced to criticize the adoption of the same PID ESTIMATOR as the SK's. We have already pointed out the inadequency of SK PID ESTIMATOR (See Galkin [1], page 6).

5 Summary

(1) The SK TDC procedure

The TDC procedure assumes that the Cherenkov light originates from a point, and thus does not determine the vertex position accurately, because the sources for the Cherenkov light have a non-negligible extent. In order to utilize the TDC meaningfully, we should take into account the extent of the source for the Cherenkov light in space and time. Further, ideally we should utilize not only arrival time of the Cherenkov light but also shape of the

pulse in the PMTs.

(2) The SK ADC procedure: the estimator for particle identification

It is no exaggeration to state that the credibility of the discrimination of muon events from electron events in the SK analysis is entirely dependent on the validity of the estimator adopted by the SK.

The estimator for particle identification was introduced into the analysis of the neutrino events in the Kamiokande detector (Takita[2]). The main purpose of the KEK 1 kiloton experiment was to test, using particles of known type and momentum, the validity of the Monte Carlo simulation used in the Kamiokande detector (Kasuga, p.22[3]). The results of this test established the validity of the estimator and thus it was applied to the standard SK analysis (Kasuga et al.[4], Sakai[5], Kasuga [3]). As a result of using this estimator, it has been asserted that evidence for neutrino oscillations between muons and tauons has been obtained.

As we have pointed out, the SK estimator for particle identification consists of three parts. The first is the probability function, in which the spatial part is separated from the angular part. The second is the probability function for photoelectron production. The third is the introduction of the point-like approximation into the Cherenkov light for electrons. As we have made clear, the first two lack a firm theoretical foundation. The third is an oversimplification which leads generally to a wrong estimation for the quantity of Cherenkov light. Consequently, the SK estimator for particle identification can not be reliable for an accurate discrimination between electrons and muons. SK results depending on the discrimination of electron-like events from muon-like events (see Kasuga et al.[4]) must be re-evaluated in this light.

(3) Errors for the vertex point and the direction

Only the correct estimator for particle identification can estimate the error for the vertex point and direction quantitatively. Our estimation (Figures 15 to 18 and Figures 19 to 22 and Table 3) shows non-negligible and inevitable errors for the vertex position and direction. It should be, particularly, noticed that the fluctuations in error in both vertex position and direction are too big.

Kibayashi (p.73[7]) concludes that the uncertainty for vertex point is from 23 cm to 56 cm and the uncertainty for the direction from 0.9° to 3.0° using both the estimator for particle identification and the TDC adopted by the SK. As we have demonstrated, these appear to severely underestimate the error distributions, which is too far from reality.

(4) In the present paper, we do not take into consideration photoelectrons produced by the Cherenkov light in the PMT, and we neglect scattering of the Cherenkov light. Therefore, our results on discrimination of electron events from muon events, only yield lower limits to the realistically achievable experimental erroes. If we consider these factors, the situation becomes much more complicated. In Figure 23, we give the Cherenkov light distributions for given numbers of photoelectron. It is easily understood from the figure that the patterns of electron events and muon events are much more vague, because there is non-negligible distribution of the photoelectron for a given number of Cherenkov photons. Further, we can say that it is quite sufficient for us to limit our analysis to the level of direct Cherenkov light, neglecting scattered Cherenkov light, to clarify the essential points in the discrimination procedure between electrons and muons.

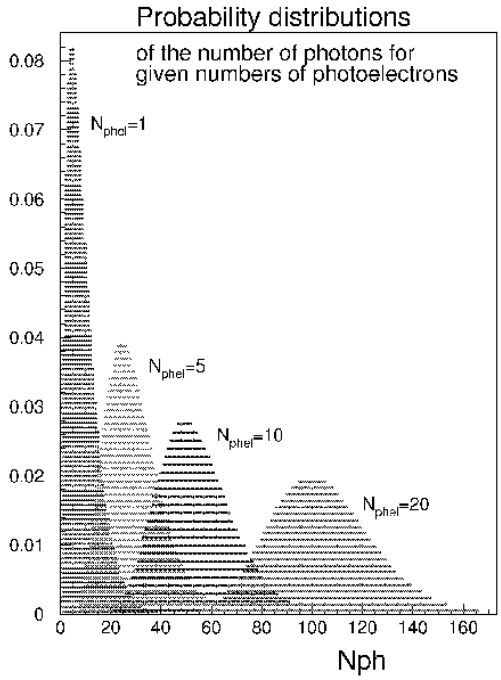

Fig. 23. Probability distributions of the number of the Cherenkov photons for given numbers of photoelectron. The number of simulation is 100.

(5) As a result of the points mentioned in (4), our results give lower limits for the primary parameter uncertainties in the problems concerned. We show a clear separation between electron and muon by using a procedure based on detailed Cherenkov light angular distribution approximations. Even though we show a clear separation between electron and muon for the same quantity of the Cherenkov light, this remains at the theoretical level and does not provide the optimal experimental means of separating electrons from muons. This problem is beyond the scope of this paper and is better undertaken by those with a detailed understanding of the specifics of the detector.

A part of the preceding paper[1] and present paper are found in [9].

6 Acknowledgement

One of the authors (V.G.) should like to thank Prof. M. Higuchi, Tohoku Gakuin University. Without his invitation, V.G. could not join in this work. Authors would like to be very grateful for the remarkable improvement of the manuscript to Dr. Philip Edwards.

References

1. Galkin,V.I.,Anokhina,A.M.,Konishi,E. and Misaki,A., Eur.Phys.J.C(submitted), arXiv:hep-ex/0412059
2. Takita,M., PhD thesis, University of Tokyo (1988)
3. Kasuga,S., ICRR Report 338-95-4 (1995)
4. Kasuga,S. *et al.*, Phys.Lett.**B374**, (1996) 238
5. Sakai,A., PhD thesis, University of Tokyo (1997)
6. Kasuga,S., PhD thesis, University of Tokyo (1998)
7. Kibayashi,A., PhD thesis, University of Hawaii (2002)
8. Mitsui,K.,Kitamura,T.,Wada,T. and Okei,K., J.Phys.G:Nucl.Part Phys.**29** (2003)2281
9. Anokhina,A.M. and Galkin,V.I.,Physics of Atomic Nuclei **69** No.1 (2006) 16